

Observing many body effects on lepton pair production from low mass enhancement and flow at RHIC and LHC energies

Sabyasachi Ghosh, Sourav Sarkar and Jan-e Alam

August 29, 2018

*Theoretical Physics Division, Variable Energy Cyclotron Centre,
1/AF, Bidhannagar, Kolkata 700064, India*

Abstract

The ρ spectral function at finite temperature calculated using the real-time formalism of thermal field theory is used to evaluate the low mass dilepton spectra. The analytic structure of the ρ propagator is studied and contributions to the dilepton yield in the region below the bare ρ peak from the different cuts in the spectral function are discussed. The space-time integrated yield shows significant enhancement in the region below the bare ρ peak in the invariant mass spectra. It is argued that the variation of the inverse slope of the transverse mass (M_T) distribution can be used as an efficient tool to predict the presence of two different phases of the matter during the evolution of the system. Sensitivity of the effective temperature obtained from the slopes of the M_T spectra to the medium effects are studied.

1 Introduction

The latest results from relativistic $Au + Au$ collisions at Relativistic Heavy Ion Collider (RHIC) have indicated that the matter created in the initial stages in relativistic heavy ion collisions (HIC) might be in the form of quark gluon plasma [1]. This is supported by the observation of high transverse momentum (p_T) hadron suppression (jet-quenching) in central collisions compared to the binary-scaled hadron-hadron interactions [2]. The observation of large elliptic flow have also indicated the possibility of rapid thermalisation of such high density matter [3].

Although the small production cross-section of lepton pairs leads to a lower yield, the electromagnetic probes are well suited to probe the local properties of the transient form of matter produced in nuclear collisions at ultra-relativistic energies as they leave the system almost unscathed. They emanate at all stages and thus are expected to map the temperature profile of the evolution. Because of the backgrounds coming from different stages and the low yield, extraction of signal from the background becomes a daunting task [4]. Theoretically, the prediction of the yield depends on the evaluation of the production rate as well as the scenario of space-time evolution that one employs. The rates of production from the QGP is controlled by QCD but those from hadronic matter depends on the hadronic interactions that one considers. In the low mass region, the rate of dilepton production is controlled by the spectral functions of the vector mesons, specially the ρ and hence the modification of the ρ spectral function determines the yield of lepton pairs in this region of invariant mass.

A number of authors have analysed the dilepton spectra from heavy ion collisions; the treatments differing both in the construction of the ρ spectral function as well as the space time evolution scenario employed. This includes the nature of phase transition, the equation of state as well as numerical values of the parameters like

the initial temperature, the thermalisation time, the phase transition temperature as well as the chemical and kinetic freeze-out temperatures. We do not attempt to review or summarise the considerable amount of work which has been done on this topic except to mention the most recent few. The NA60 experiment at the CERN SPS measured dimuon pairs in In-In collisions in which an excess was observed over the contribution from hadronic decays at freeze-out in the mass region below the ρ peak [4]. This was attributed to the broadening of the ρ in hot and dense medium [5], in contrast to the earlier data from the CERES collaboration [6] which is unable to differentiate between the broadening and the pole shift of the ρ spectral function [7]. The NA60 data for the entire (measured) invariant mass range is reproduced by taking into account dilepton productions from Drell-Yan processes, $q\bar{q}$ annihilation, thermally broadened in-medium ρ , decays of ρ at the freeze-out surface and primordial ρ produced from the initial hard scattering [8]. The dependence of thermal emission on transition and chemical freeze-out temperatures is also highlighted there. The dilepton yield evaluated with the in-medium spectral functions of ρ and ω mesons deduced from empirical forward scattering amplitudes [9] does not reproduce the data well at the low invariant mass ($M < 0.5$ GeV) region. The PHENIX experiment reported a substantial excess of electron pairs in the same region of invariant mass [10]. The data has been investigated by several groups e.g. [11, 12]. The yield in all these cases have remained insufficient to explain the PHENIX data [13]. Thus the issue of low mass lepton pair yield still remains an unsettled issue.

In the literature the modification of the ρ propagator comes from (a) the thermal modification of the decay width into pion pairs and (b) collisional broadening due to scattering with the excitations in the thermal medium [5]. In this work we have studied dilepton production at RHIC and LHC (Large Hadron Collider) energies using a spectral function evaluated in the real time formulation of thermal field theory with the interaction vertices taken from chiral perturbation theory which is the low energy effective theory of QCD. From the discontinuities of the ρ self energy associated with the branch cuts in the complex energy plane we provide a unified description of the apparently different scattering and decay processes in the medium [14] (for a different approach see [15, 5]). The resulting spectral function of the ρ at non-zero three-momentum shows significant broadening with no appreciable change in the pole position. Since the dilepton spectra is proportional to the vector meson spectral function, the ρ in particular, we will attempt to bring out the medium modifications through different aspects of the dilepton spectra (see [5, 16] for review).

For the space-time evolution we have used ideal relativistic hydrodynamics. There are quite a few parameters which go as inputs into this scheme e.g. the thermalisation time or the initial temperature. Though studies on elliptic flow of matter produced in such collisions indicate a rapid thermalisation [17], analyses using second order transport coefficients with conformal symmetry indicate sizable uncertainties [18] in its determination. Then comes the issue of transition temperature in addition to the chemical and kinetic freeze-out temperatures. The equation of state, in particular the velocity of sound is another vital input which goes into the hydrodynamics and control the evolution profile. Since electromagnetic probes are emitted throughout the spatial and temporal extent of the fireball, the spectra is in fact sensitive to each of these factors. We will investigate the dependence of the dilepton spectra in the low mass region on the equation of state (EoS) obtained from two different schemes.

It is well known that the average magnitude of radial flow at the freeze-out surface can be extracted from the p_T spectra of various hadrons. However, hadrons being strongly interacting objects can bring the information of the state of the system when it is too dilute to support collectivity *i.e.* the parameters of collectivity extracted from the hadronic spectra are limited to the evolution stage where the collectivity ceases to exist. These collective parameters have hardly any information about the interior of the matter. On the other hand dileptons (and real photons) are produced and emitted from each space time point. Again, dileptons have an additional advantage because in this case we have two kinematic variables - of these, the p_T spectra is affected by the flow in the system but the p_T integrated invariant mass (M) spectra remains unaltered. Therefore, if one can identify a domain of M where QGP contributions dominate then the flow from the interior of the

QGP phase may be extracted by studying the M_T spectra at this M window *i.e.* a judicious choice of p_T and M windows will be very useful to characterise the flow in QGP and hadronic phases, which will shed light on the time evolution of the collectivity in the system [19]. The effective slope of the dilepton spectra have been extracted both for the RHIC and LHC energies to demonstrate these aspects.

In this work we have thus focused on two kinds of many body effects which are inherent in the evaluation of dilepton spectra from heavy ion collisions. The one concerning the in-medium vector meson spectral function is microscopic in nature originating from the dynamics of effective hadronic interactions taken from chiral perturbation theory and the other is a macroscopic manifestation which results in collective flow of the fireball described by relativistic hydrodynamics. Both of these effects can be observed by studying the low mass lepton pairs with appropriate choice of invariant mass and transverse momentum windows. We demonstrate this by evaluating the lepton pair spectra for RHIC and LHC conditions.

The organisation of the paper is as follows. In section 2 we shall discuss the details of calculation of the spectral function of vector mesons and subsequently the differential dilepton rate. Space-time evolution of the evolving matter will be discussed in section 3. Space-time integrated dilepton yields are presented in section 4 and finally we conclude in section 5.

2 Dilepton emission rate

The rate of dilepton production rate from a thermal medium produced in heavy ion collisions is well known to be given by [20]

$$\frac{dN}{d^4q d^4x} = -\frac{\alpha^2}{6\pi^3 q^2} L(M^2) f_{BE}(q_0) g^{\mu\nu} W_{\mu\nu}(q_0, \vec{q}) \quad (1)$$

where the factor $L(M^2) = (1 + 2m_l^2/M^2) (1 - 4m_l^2/M^2)^{1/2}$ is of the order of unity for electrons, $M(= \sqrt{q^2})$ being the invariant mass of the pair and the electromagnetic (e.m.) current correlator $W_{\mu\nu}$ is defined by

$$W_{\mu\nu}(q_0, \vec{q}) = \int d^4x e^{iq \cdot x} \langle [J_\mu^{em}(x), J_\nu^{em}(0)] \rangle \quad (2)$$

Here $J_\mu^{em}(x)$ is the electromagnetic current and $\langle \rangle$ indicates ensemble average. For a deconfined thermal medium such as the QGP, Eq. (1) leads to the standard rate for lepton pair production from $q\bar{q}$ annihilation [21] at lowest order.

At low values of the invariant mass M , the electromagnetic current of quarks $J_\mu^{em} = \frac{2}{3}\bar{u}\gamma_\mu u - \frac{1}{3}\bar{d}\gamma_\mu d - \frac{1}{3}\bar{s}\gamma_\mu s$ may be decomposed as

$$J_\mu^{em} = J_\mu^\rho + J_\mu^\omega/3 - J_\mu^\phi/3 \quad (3)$$

where the vector currents

$$\begin{aligned} J_\mu^\rho &= \frac{1}{2}(\bar{u}\gamma_\mu u - \bar{d}\gamma_\mu d) \\ J_\mu^\omega &= \frac{1}{2}(\bar{u}\gamma_\mu u + \bar{d}\gamma_\mu d) \\ J_\mu^\phi &= \bar{s}\gamma_\mu s \end{aligned} \quad (4)$$

are named by the lowest mass hadrons ρ^0 , ω and ϕ in the corresponding channel. Defining the correlator of these currents $W_{\mu\nu}^{\rho,\omega,\phi}$ analogously as in (2) we write,

$$W_{\mu\nu} = W_{\mu\nu}^\rho + W_{\mu\nu}^\omega/9 + W_{\mu\nu}^\phi/9. \quad (5)$$

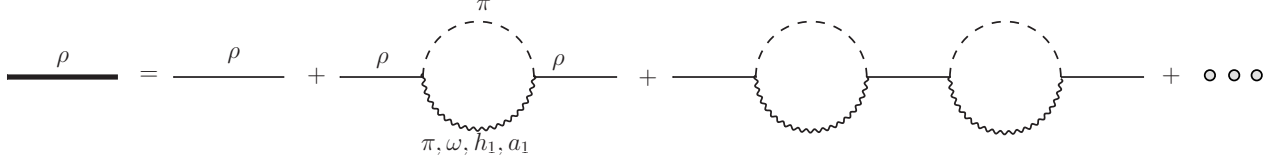


Figure 1: The Dyson equation for the ρ propagator, the small circles indicating terms of higher order in the series.

One now has to specify the coupling of the currents to the corresponding vector fields. For this purpose we write, in the narrow width approximation [22],

$$\langle 0 | J_\mu^{em}(0) | R \rangle = F_R m_R \epsilon_\mu \quad (6)$$

where R denotes the resonance in a particular channel and ϵ_μ is the corresponding polarisation vector. The coupling constants F_R are obtained from the partial decay widths into e^+e^- through the relation

$$F_R^2 = \frac{3m_R \Gamma_{R \rightarrow e^+e^-}}{4\pi\alpha^2} \quad (7)$$

yielding $F_R=0.156$ GeV, 0.046 GeV and 0.079 GeV for ρ , ω and ϕ respectively. Eq. (6) suggests the operator relations

$$J_\mu^\rho(x) = F_\rho m_\rho V_\mu^\rho(x), \quad J_\mu^\omega(x) = 3F_\omega m_\omega V_\mu^\omega(x) \text{ etc.} \quad (8)$$

where $V_\mu^{\rho(\omega)}(x)$ denotes the field operator for the $\rho(\omega)$ meson. The vector correlator in the ρ channel for example, is then given by

$$\begin{aligned} W_{\mu\nu}^\rho &= F_\rho^2 m_\rho^2 \int d^4x e^{iq \cdot x} \langle [V_\mu^\rho(x), V_\nu^\rho(0)] \rangle \\ &= K_\rho \rho_{\mu\nu}^\rho(q_0, \vec{q}) \end{aligned} \quad (9)$$

where $\rho_{\mu\nu}^\rho$ is the spectral function of the ρ meson in the thermal medium and $K_\rho = F_\rho^2 m_\rho^2$. Defining the spectral functions of ω and ϕ as in (9), the dilepton rate is given by

$$\frac{dN}{d^4q d^4x} = -\frac{\alpha^2}{6\pi^3 q^2} f_{BE}(q_0) g^{\mu\nu} [K_\rho \rho_{\mu\nu}^\rho(q_0, \vec{q}) + K_\omega \rho_{\mu\nu}^\omega(q_0, \vec{q}) + K_\phi \rho_{\mu\nu}^\phi(q_0, \vec{q})] \quad (10)$$

2.1 Spectral function in terms of self energy

The ρ meson plays the most significant role in the low mass region. We thus begin with the complete ρ propagator which in the real time formulation of thermal field theory is a 2×2 matrix defined by

$$D_{\mu\nu}^{ab}(q_0, \vec{q}) = i \int d^4x e^{iq \cdot x} \langle \mathcal{T}_c V_\mu^\rho(x) V_\nu^\rho(0) \rangle^{ab} \quad (11)$$

where the superscripts $(a, b = 1, 2)$ are thermal indices and \mathcal{T}_c denotes time ordering with respect to a contour in the complex time plane. In the case of a symmetric contour this matrix function factorises as [23]

$$D_{\mu\nu}^{ab} = U \begin{pmatrix} \bar{D}_{\mu\nu} & 0 \\ 0 & -\bar{D}_{\mu\nu}^* \end{pmatrix} U; \quad U = \begin{pmatrix} \sqrt{1+n} & \sqrt{n} \\ \sqrt{n} & \sqrt{1+n} \end{pmatrix} \quad (12)$$

and so is given essentially by a single analytic function, the diagonal component $\overline{D}_{\mu\nu}$. This function admits a Kallen Lehmann representation given by [24]

$$\overline{D}_{\mu\nu}(q_0, \vec{q}) = \int_{-\infty}^{\infty} \frac{dq'_0}{2\pi} \frac{\rho_{\mu\nu}^{\rho}(q'_0, \vec{q})}{q'_0 - q_0 - i\eta\epsilon(q_0)} \quad (13)$$

in terms of the spectral function defined in Eq. (9). From this we obtain

$$\rho_{\mu\nu}^{\rho}(q_0, \vec{q}) = 2\epsilon(q_0)\text{Im}\overline{D}_{\mu\nu}(q_0, \vec{q}) \quad (14)$$

Thus the dilepton rate is essentially given by the imaginary part of the ρ propagator which we will now elaborate in the following.

The complete ρ propagator in the medium is obtained from the Dyson equation

$$D_{\mu\nu}^{ab}(q) = D_{\mu\nu}^{(0)ab}(q) - D_{\mu\lambda}^{(0)ac}(q)\Pi^{cd,\lambda\sigma}(q)D_{\sigma\nu}^{db}(q) \quad (15)$$

pictorially seen in Fig. 1. $D_{\mu\nu}^{(0)ab}(q)$ is the free thermal propagator and $\Pi_{\mu\nu}^{ab}(q)$ denotes self energy insertions both of which are 2×2 matrices in this approach. Here we have considered one-loop diagrams consisting of a pion and another hadron h where h stands for π, ω, a_1, h_1 mesons restricting thus to the non-strange meson sector. These self energy graphs provide corrections to the ρ meson propagation in the medium and will be evaluated in the next section.

One can get rid of the thermal indices on diagonalising the thermal propagator and self energy matrices so that Eq. (15) now takes the form

$$\overline{D}_{\mu\nu}(q) = \overline{D}_{\mu\nu}^{(0)}(q) - \overline{D}_{\mu\lambda}^{(0)}(q)\overline{\Pi}^{\lambda\sigma}(q)\overline{D}_{\sigma\nu}(q) \quad (16)$$

the bars denoting the diagonal components as discussed above. $\overline{D}_{\mu\nu}^{(0)}(q)$ turns out to be the vacuum propagator given by

$$\overline{D}_{\mu\nu}^{(0)}(q) = \left(-g_{\mu\nu} + \frac{q_{\mu}q_{\nu}}{m_{\rho}^2} \right) \frac{-1}{q^2 - m_{\rho}^2 + i\epsilon} \quad (17)$$

The complete propagator $\overline{D}_{\mu\nu}(q)$ can be obtained in terms of transverse and longitudinal components by writing

$$\overline{D}_{\mu\nu} = P_{\mu\nu}\overline{D}_t + Q_{\mu\nu}\overline{D}_l \quad (18)$$

and

$$\overline{\Pi}_{\mu\nu} = P_{\mu\nu}\overline{\Pi}_t + Q_{\mu\nu}\overline{\Pi}_l \quad (19)$$

where the projection operators are given by

$$P_{\mu\nu} = -g_{\mu\nu} + \frac{q_{\mu}q_{\nu}}{q^2} - \frac{q^2}{\vec{q}^2}\tilde{u}_{\mu}\tilde{u}_{\nu}, \quad Q_{\mu\nu} = \frac{(q^2)^2}{\vec{q}^2}\tilde{u}_{\mu}\tilde{u}_{\nu}, \quad \vec{q}^2 = (u \cdot q)^2 - q^2, \quad (20)$$

u_{μ} being four-velocity of the heat bath and $\tilde{u}_{\mu} = u_{\mu} - u \cdot q q_{\mu}/q^2$. Using these in Eq. (16) we eventually arrive at the solutions

$$\overline{D}_t(q) = \frac{-1}{q^2 - m_{\rho}^2 - \overline{\Pi}_t(q)}, \quad \overline{D}_l(q) = \frac{1}{q^2} \frac{-1}{q^2 - m_{\rho}^2 - q^2\overline{\Pi}_l(q)} \quad (21)$$

neglecting the non-transverse piece in $\overline{D}_{\mu\nu}^{(0)}(q)$. These are used in Eqs. (14) and (10) to arrive at the dilepton emission rate

$$\frac{dN}{d^4q d^4x} = \frac{\alpha^2}{\pi^3 q^2} f_{BE}(q_0) [K_{\rho}A_{\rho}(q_0, \vec{q}) + K_{\omega}A_{\omega}(q_0, \vec{q}) + K_{\phi}A_{\phi}(q_0, \vec{q})]. \quad (22)$$

where e.g. $A_\rho (= -g^{\mu\nu} \rho_{\mu\nu}^\rho(q_0, \vec{q})/6)$ is given by

$$A_\rho = -\frac{1}{3} \left[\frac{2 \sum \text{Im} \Pi_t^R}{(q^2 - m_\rho^2 - \sum \text{Re} \Pi_t^R)^2 + (\sum \text{Im} \Pi_t^R)^2} + \frac{q^2 \sum \text{Im} \Pi_t^R}{(q^2 - m_\rho^2 - q^2 \sum \text{Re} \Pi_t^R)^2 + q^4 (\sum \text{Im} \Pi_t^R)^2} \right] \quad (23)$$

the sum running over the $\pi - h$ loops. Thus, the dilepton emission rate in the present scenario boils down to the evaluation of the self energy graphs shown in Fig. 1. The real and imaginary parts of the self energy function can be obtained from the 11-component as [23]

$$\begin{aligned} \text{Re} \Pi_{\mu\nu}^R(q_0, \vec{q}) &= \text{Re} \bar{\Pi}_{\mu\nu}(q_0, \vec{q}) = \text{Re} \Pi_{\mu\nu}^{11}(q_0, \vec{q}) \\ \text{Im} \Pi_{\mu\nu}^R(q_0, \vec{q}) &= \epsilon(q_0) \text{Im} \bar{\Pi}(q_0, \vec{q}) = \tanh(\beta q_0/2) \text{Im} \Pi_{\mu\nu}^{11}(q_0, \vec{q}) \end{aligned} \quad (24)$$

where Π^R denotes the retarded self-energy.

2.2 Evaluation of ρ self energy

A. Hot meson gas

The 11-component of the thermal self-energy matrix for the $\pi - h$ loops is given by

$$\Pi_{\mu\nu}^{11}(q) = i \int \frac{d^4 k}{(2\pi)^4} N_{\mu\nu}(q, k) D_\pi^{11}(k) D_h^{11}(q - k), \quad (25)$$

where $D^{11}(q)$ are the thermal propagators [24] and the factor $N_{\mu\nu}$ includes tensor structures associated with the two vertices and those in the vector propagator. In Ref. [14], this was evaluated in detail using interaction vertices from chiral perturbation theory to obtain the imaginary part of the retarded ρ self energy. For positive values of q_0 this is given by

$$\begin{aligned} \text{Im} \Pi_{\rho\pi}(q_0, \vec{q}) &= -\pi \int \frac{d^3 \vec{k}}{(2\pi)^3 4\omega_\pi \omega_h} \times \\ &[N(k_0 = \omega_\pi)(1 + n(\omega_\pi) + n(\omega_h))\delta(q_0 - \omega_\pi - \omega_h) + N(k_0 = -\omega_\pi)(n(\omega_\pi) - n(\omega_h))\delta(q_0 + \omega_\pi - \omega_h)] \end{aligned} \quad (26)$$

where n is the Bose distribution function and the energy variables are $\omega_\pi = \sqrt{m_\pi^2 + \vec{k}^2}$, $\omega_h = \sqrt{m_h^2 + (\vec{q} - \vec{k})^2}$. Here we have suppressed indices corresponding to the longitudinal and transverse components which have been evaluated as in [14]. We recall that the regions in the q_0 plane in which the two terms are non-vanishing give rise to cuts in the self energy function. These are controlled by the corresponding delta functions. The first term is non-vanishing for $q^2 \geq (m_h + m_\pi)^2$ producing the unitary cut and the second term is non-vanishing for $q^2 \geq (m_h - m_\pi)^2$ giving the Landau cut. The unitary cut is also present in vacuum but the Landau cut appears only in the medium and arises from scattering of ρ with the particles present there. With the aid of the delta functions the integration over \vec{k} is easily performed.

Note that the heavy mesons in [14] have been treated in the narrow width approximation. In the following we consider the conventional prescription (see e.g. [25]) to take into account the decay widths of the h_1 and a_1 mesons without disturbing the analytic structure discussed above. Here, the self energy functions are convoluted with the (vacuum) spectral functions of the heavy mesons (h) as

$$\Pi(q, m_h) = \frac{1}{N_h} \int_{(m_h-2\Gamma_h)^2}^{(m_h+2\Gamma_h)^2} d\tilde{m}_h^2 \frac{1}{\pi} \text{Im} \frac{1}{\tilde{m}_h^2 - m_h^2 + i\tilde{m}_h\Gamma(\tilde{m}_h)} \Pi(q, \tilde{m}_h) \quad (27)$$

with

$$N_h = \int_{(m_h-2\Gamma_h)^2}^{(m_h+2\Gamma_h)^2} d\tilde{m}_h^2 \frac{1}{\pi} \text{Im} \frac{1}{\tilde{m}_h^2 - m_h^2 + i\tilde{m}_h\Gamma(\tilde{m}_h)} \quad (28)$$

where Γ_h are the measured [26] decay widths and $\Gamma(\sqrt{s} = \tilde{m}_h)$ are the corresponding ones calculated using hadronic interactions. As a consequence of this convolution the clear distinction between the regions of non-zero imaginary part will be smeared and for sufficiently large width might even appear continuous. However, for a particular value of the mass \tilde{m}_h , the imaginary part receives contribution from only one of the cuts.

B. Effect of baryons

It is known that the scattering of the ρ with baryons also contribute to the broadening of its spectral function even in the case of zero baryon density, and thereby increase the production of lepton pairs at invariant masses below the ρ peak. The relevant quantity in this case is the ρ self-energy due to baryon loops which has been evaluated at finite temperature and density using well established hadronic interactions in a many body approach [27].

The ρ self-energy at finite temperature and baryon density has also been estimated in terms of empirical scattering amplitudes [28] for ρ scattering from nucleons using experimental data. The self energy of the ρ is obtained from these amplitudes using a low density approximation as

$$\Pi_{\rho N}(E, p) = -4\pi \int \frac{d^3k}{(2\pi)^3} n_B(\omega) \frac{\sqrt{s}}{\omega} f_{\rho N}^{c.m.}(s) \quad (29)$$

The scattering amplitude $f_{\rho N}^{c.m.}(s)$ in the low energy region is described in terms of N^* and Δ baryon resonances and a Regge model is employed at higher energies [28]. Since the spectral function in this approach seems to agree with the many body approach as shown in [29] we will adopt this formalism to estimate the baryonic contribution to the self energy.

The total ρ self energy in hadronic matter containing mesons and baryons is then written as

$$\Pi_\rho = \Pi_{\rho h} + \Pi_{\rho N} . \quad (30)$$

The spectral function as a function of M is plotted in Fig. 2 for a range of temperatures at a baryonic chemical potential $\mu_B = 30$ MeV relevant for RHIC energies. We observe significant broadening at higher temperatures with almost negligible shift in the pole mass.

2.3 The dilepton emission rate at temperature T

We next plot in Fig. 3, upper panel, the dilepton emission rate keeping only the ρ contribution in Eq. (22) in which we show, for illustrative purposes, the relative contributions from the cuts in the $\pi - h$ loops keeping only one of them at a time. The unitary and Landau cuts for the π, ω, h_1 and a_1 are seen to contribute with different magnitudes for different values of the energy and three momenta of the off-shell ρ . In the time-like region, in the vicinity of the (bare) rho mass the imaginary part of the self energy from a particular loop receives dominant contribution from only one of the cuts. The $\pi - \pi$ loop for example, has only the unitary cut and this contributes most significantly to dilepton emission near the ρ pole. In contrast, the Landau cut contribution from the $\pi - \omega$ loop is dominant up to about 400 MeV. Since this cut ends at $M = m_\omega - m_\pi$ and the unitary cut starts at $M = m_\omega + m_\pi$ there is no contribution at the ρ pole. However, the unitary cut of the

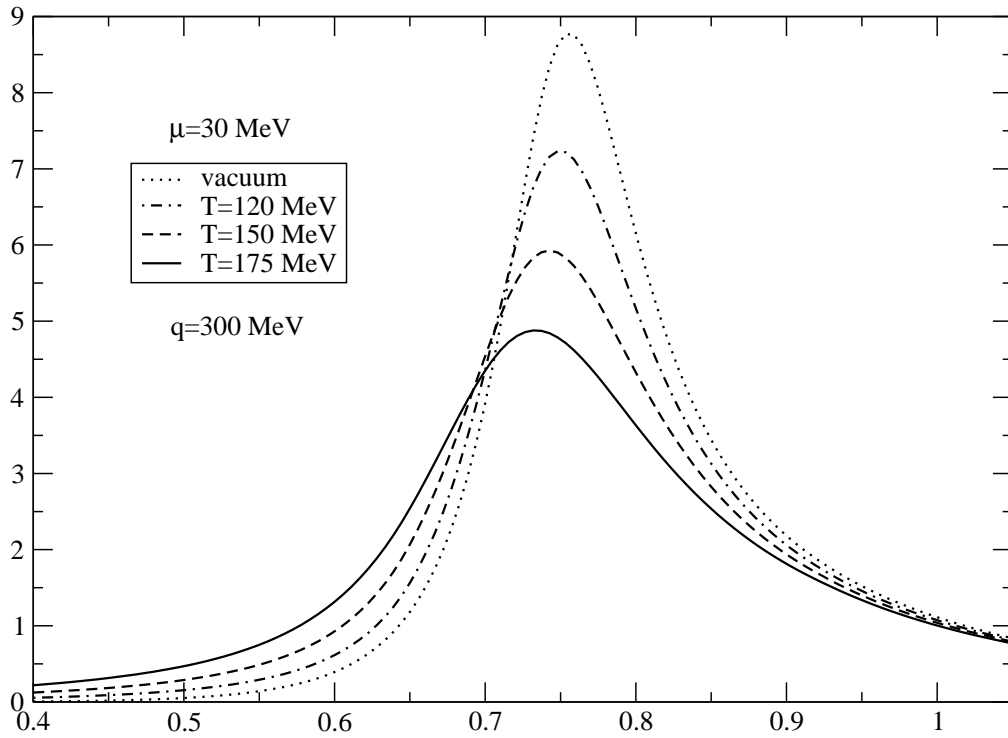


Figure 2: The ρ spectral function averaged over the transverse and longitudinal polarisations for $\vec{q}=300 \text{ MeV}$ and $\mu_B = 30 \text{ MeV}$.

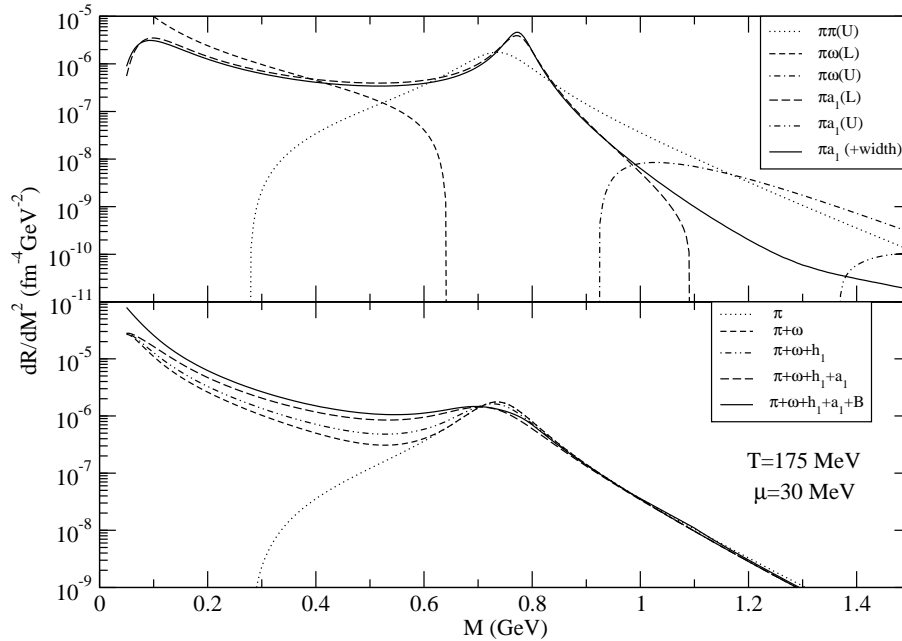


Figure 3: Upper panel shows contributions from the discontinuities of the self-energy graphs to the dilepton emission rate at $T = 175$ MeV and $\mu_B = 30$ MeV. L and U denote the Landau and unitary cut contribution. Lower panel shows contributions from the mesons and baryons.

$\omega\pi$ loop could make a significant contribution as seen in [14, 30]. The Landau cut for the $\pi - a_1$ self-energy extends up to about 1100 MeV and makes a substantial contribution both at and below the ρ pole. The unitary cut starts at a much higher value of M and hence does not make a significant contribution to the ρ spectral function. We also show the effect of convolution over the width of the a_1 as discussed above. As expected, the contributions from the Landau and unitary cuts are now joined by a continuous line, the boundaries being smeared out due to the substantial width of the a_1 . While analysing the different contributions one must keep in mind that the total contribution from the different loops to the spectral function is not a linear sum of the individual contributions as is clear from the definition given in Eq. (23). This is seen in the lower panel where the cumulative contribution to the lepton pair yield is shown for the $\pi - \pi$ and $\pi - h$ loops. Also shown is the enhancement in yield obtained by including baryons at $\mu_B = 30$ MeV for RHIC energies.

We have also included dilepton emission from the ω and the ϕ . The width of the ω at finite temperature is taken from the calculation of Ref [31] where a framework similar to the one employed here has been used. For the ϕ only the vacuum width has been considered. In addition, the spectral function of the ρ and ω has been augmented with a continuum contribution given by

$$\frac{dN}{d^4q d^4x} = \frac{\alpha^2}{\pi^3} f_{\text{BE}}(q_0) \sum_{V=\rho,\omega} A_V^{\text{cont}} \quad (31)$$

where the continuum part is parametrised as [16, 22]

$$A_\rho^{\text{cont}} = \frac{1}{8\pi} \left(1 + \frac{\alpha_s}{\pi}\right) \frac{1}{1 + \exp(\omega_0 - q_0)/\delta} \quad (32)$$

with $\omega_0 = 1.3$ (1.1) for ρ (ω) GeV and $\delta = 0.2$ for for both ρ and ω . The continuum contribution for the ω contains an additional factor of 1/9. The dilepton emission rates from QGP and hadronic matter have been

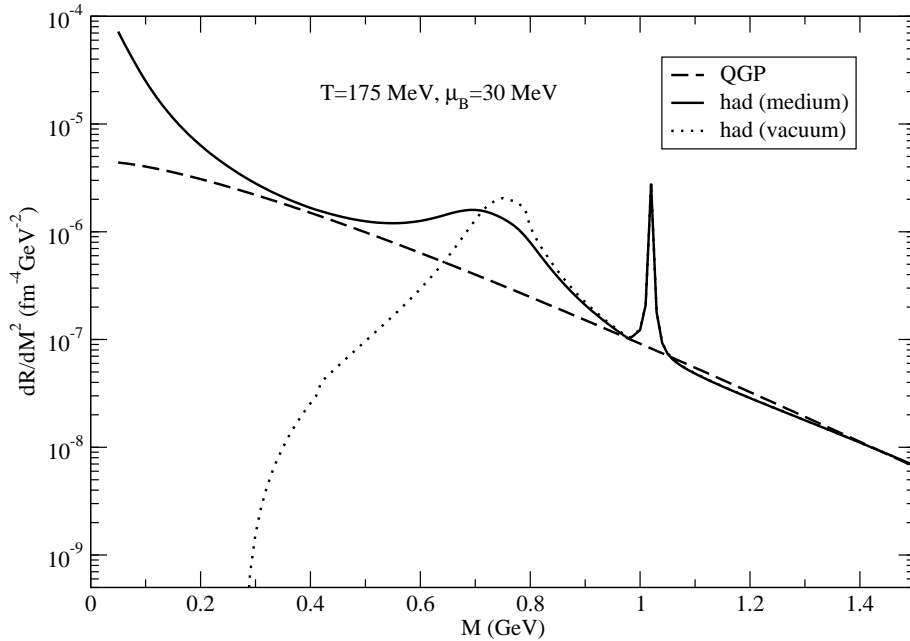


Figure 4: The dilepton emission rate from different sources at $T = 175$ MeV and $\mu_B = 30$ MeV.

plotted in Fig. 4 at a temperature of 175 MeV and baryonic chemical potential of 30 MeV. We observe significant enhancement in the dilepton yield in the mass region below the ρ pole compared to vacuum. This rate has been used in the analysis of the dimuon spectra obtained from In-In collisions at 17.3 GeV at CERN SPS [32]. The calculations show a reasonable agreement with the invariant mass spectra for different p_T ranges as well as the M_T spectra for different M bins.

3 Space time evolution

Thus far we have discussed the dilepton emission rates for a given temperature. In a HIC the temperature corresponds to that of local equilibrium and is hence a function of position and time. For a quantitative evaluation of the dilepton yield one has to convolute the static rate over space and time resulting in an integrated yield which is a superposition of contributions from a range of temperatures. Ideal relativistic hydrodynamics is used to carry out this scheme in which a number of inputs are required. These are discussed in the following.

3.1 Equation of state and initial conditions

The evolution of the fluid is governed by the energy momentum conservation equation

$$\partial_\mu T^{\mu\nu} = 0 \quad (33)$$

where $T^{\mu\nu} = (\epsilon + P)u^\mu u^\nu + g^{\mu\nu}P$ is the energy momentum tensor for ideal fluid. This together with a relation connecting the pressure P and the energy density ϵ , known as the EoS provides a closed set of equations [33]. With cylindrical symmetry and longitudinal boost invariance [34], these set of equations provide the energy density and transverse velocity as a function of the proper time and the radial coordinate. The initial energy

density and radial velocity profiles which go as inputs are taken as:

$$\epsilon(\tau_i, r) = \frac{\epsilon_0}{1 + e^{(r-R_A)/\delta}} \quad (34)$$

and

$$v(\tau_i, r) = 0 \quad (35)$$

δ (~ 0.5 fm here) is a parameter, known as the surface thickness. The static rate, dR/dM^2 at $M = 0.4$ GeV with $\mu_B = 30$ MeV and $\mu_B = 0$ differs by less than 10%. The difference will be even smaller at LHC energies because of the smaller value of μ_B at central rapidity region. Therefore, the effects of μ_B on space-time evolution is neglected in the present work.

It is natural to expect that different EoS's will govern the hydrodynamic flow quite differently [17] and as far as the search for QGP is concerned, the goal is to look for distinctions in the observables due to the different EoS's (corresponding to the novel state of QGP vis-a-vis that for the usual hadronic matter). It is thus imperative to understand in what respects the two EoS's differ and how they affect the evolution in space and time. In order to check sensitivity with the equation of state (EoS), we have considered two scenarios: (a) hadronic resonance gas (HRG) with all hadrons up to mass 2.5 GeV for the hadronic phase along with a bag model EoS for the QGP phase and (b) EoS obtained from lattice QCD calculations (LQCD) [35].

One of the most important parameters that go into the space time evolution are the values of the initial temperature and the thermalisation time. There are indications that QGP thermalises quite early at RHIC energies. In case of isentropic expansion the experimentally measured hadron multiplicity can be related to the initial temperature and thermalisation time by the following equation [36]:

$$T_i^3(b_m)\tau_i = \frac{2\pi^4}{45\zeta(3)\pi R_\perp^2 4a_k} \langle \frac{dN}{dy}(b_m) \rangle \quad (36)$$

where $\langle dN/dy(b_m) \rangle$ is the hadron (predominantly pion) multiplicity for a given centrality class with maximum impact parameter b_m . R_\perp is the transverse dimension of the system, τ_i is the initial thermalisation time, $\zeta(3)$ is the Riemann zeta function and $a_k = (\pi^2/90) g_k$ is related to the degeneracy (g_k) of the system created. The hadron multiplicity resulting from $Au + Au$ collisions is related to that from pp collisions at a given impact parameter and collision energy by

$$\langle \frac{dN}{dy}(b_m) \rangle = [(1-x)\langle N_{part}(b_m) \rangle / 2 + x\langle N_{coll}(b_m) \rangle] \frac{dN_{pp}}{dy} \quad (37)$$

where x is the fraction of hard collisions, $\langle N_{part} \rangle$ and $\langle N_{coll} \rangle$ are the average numbers of participants and collisions respectively evaluated by using Glauber model. $dN_{pp}^{ch}/dy = 2.5 - 0.25\ln(s) + 0.023\ln^2 s$, is the multiplicity of the produced hadrons in pp collisions at centre of mass energy, \sqrt{s} [37]. Assuming 10% hard (i.e. $x = 0.10$) and 90% soft collisions for initial entropy production the value of dN_{pp}^{ch}/dy turns out to be about 2.43 at $\sqrt{s} = 200$ GeV. For RHIC energy, we take $T_i = 320$ MeV with initial time $\tau_i = 0.2$ fm/c which acts as inputs to the hydrodynamic evolution.

At LHC the measured values of dN_{pp}^{ch}/dy for $\sqrt{s_{NN}} = 900$ GeV, 2.36 TeV and 7 TeV are 3.02, 3.77 and 6.01 respectively [38]. The value dN_{pp}^{ch}/dy at $\sqrt{s_{NN}} = 5.25$ TeV is obtained by interpolating the above experimental data mentioned above. Assuming $x = 0.2$ in Eq. (37) we obtain $dN/dy = 2607$ in Pb+Pb collision for 0-10% centrality. For $\tau_i = 0.1$ fm/c we get $T_i = 686$ MeV.

For the space-time picture, we thus work in the following scenario. An equilibrated QGP is formed at initial temperature (time) $T_i(\tau_i)$, the system then cools due to expansion and when the temperature reaches T_c it undergoes a phase transition from QGP to hadrons. After the completion of the phase transition the

hadronic matter cools and eventually freezes out first chemically at a temperature T_{ch} and then kinetically at a temperature T_F . The transition temperature is taken as $T_c \sim 175$ MeV. The other inputs which goes into the calculations are chemical (T_{ch}) and kinetic freeze-out (T_F) temperatures. The kinetic freeze-out in the system occurs when both the elastic and in-elastic collisions stop i.e. the freeze-out takes place when the collectivity in the system ceases to exist. The value of T_F can be constrained from the hadronic p_T spectra [1]. In the present work we take $T_F = 120$ MeV which reproduces the p_T spectra of pions, kaons reasonably well [39]. The ratios of various hadrons measured experimentally at different $\sqrt{s_{NN}}$ indicate that the system formed in heavy ion collisions chemically decouple at T_{ch} which is higher than T_F [40]. Therefore, the system remains out of chemical equilibrium from T_{ch} to T_F . The deviation of the system from the chemical equilibrium is taken in to account by introducing chemical potential for each hadronic species [41]. The chemical non-equilibration affects the yields through the phase space factors of the hadrons which in turn affects the productions of the EM probes. The chemical potential, μ_j for the hadronic species j as a function of T have been taken from Ref. [42]:

$$\frac{n_j(T, \mu_j)}{s(T, \{\mu_j\})} = \frac{n_j(T_{ch}, \mu_j = 0)}{s(T_{ch}, \{\mu_j\} = 0)} \quad (38)$$

where n_j is the density of hadron j contains direct as well as contributions from resonance decays. The μ_j is a function of T and it vanishes at $T = T_{ch}$ ($= 170$ MeV here). Therefore, the space time evolution of μ_j is dictated by the evolution of T . The chemical potentials of pions, ω , h_1 , a_1 , ϕ and proton enters through their thermal distributions as a fugacity factor. The values of the respective chemical potential at the kinetic freeze-out temperature, $T_F = 120$ MeV are $\mu_\pi = 68$ MeV, $\mu_\omega = 179$ MeV, $\mu_{h_1} = 204$ MeV $\mu_{a_1} = 204$ MeV, $\mu_\phi = 252$ MeV $\mu_{proton} = 258$ MeV.

We have also included the contribution to the dilepton yield from the decays of ρ mesons at freeze-out using the Cooper-Frye formula [43] as follows. For a special case of unstable vector mesons we need to know the thermal phase space factor corresponding to an unstable Boson which is given by

$$f_{\text{unstable}} = \frac{g}{(2\pi)^3} \int \frac{1}{\exp(E/T) - 1} A_\rho(M) dM^2 \quad (39)$$

where $E = \sqrt{p^2 + M^2}$, g is the statistical degeneracy and $A_\rho(M)$ is the (vacuum) spectral function of the vector meson under consideration. For stable particle $A_\rho(M)$ reduces to a Dirac delta function and consequently the usual phase space factor for a stable particle is recovered upon integration over dM^2 . Therefore, the m_T distribution of dimuons from vector meson decay after the freeze-out is given by [8] (see also [44]):

$$\begin{aligned} \frac{dN_{\gamma^*}}{M_T dM_T dM^2 dy} &= 2\pi \int dr \int d\eta \int d\phi r \tau \\ &\times \left(M_T \cosh(y - \eta) - \frac{\partial \tau}{\partial r} p_T \cos \phi \right) \\ &\times f_{\text{unstable}} \Gamma_{V \rightarrow \mu^+ \mu^-} / \Gamma_V^{\text{tot}} \end{aligned} \quad (40)$$

where Γ_V^{tot} is the total decay width of the vector meson V .

4 Dilepton spectra at RHIC and LHC

We begin by plotting the space-time integrated invariant mass spectra of dileptons. In Fig. 5 we plot the yield of lepton pairs from the hadronic matter (HM) containing the effects of chemical non-equilibration both in

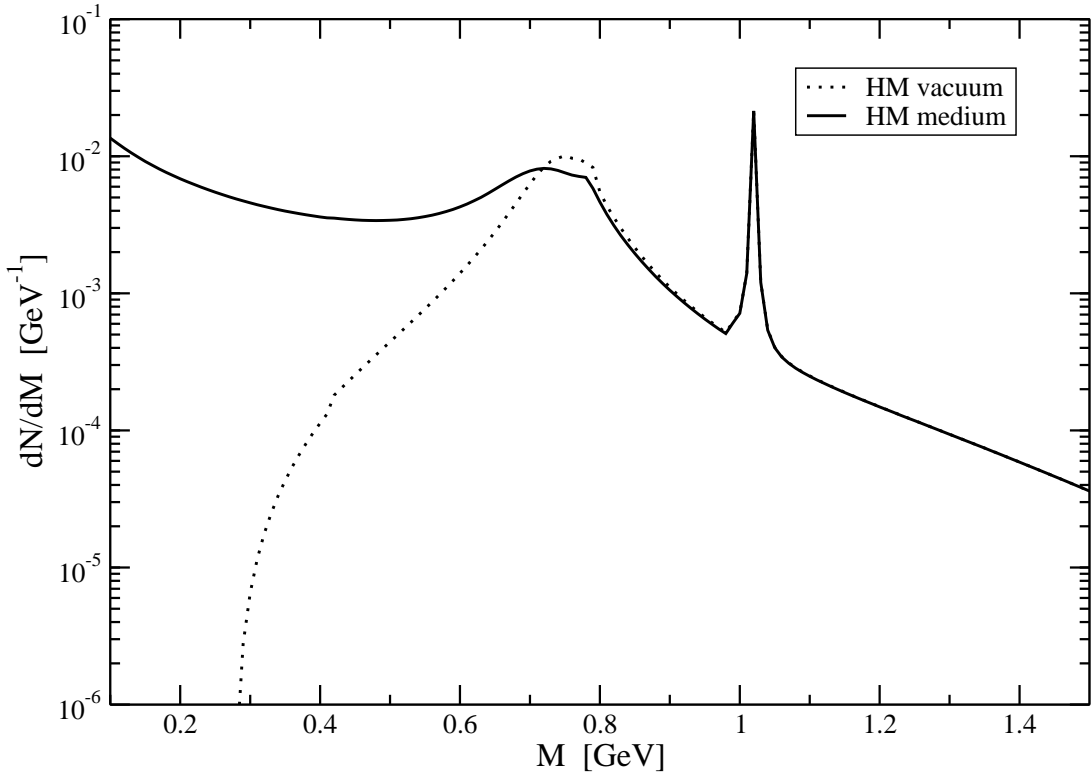


Figure 5: Invariant mass distribution of dileptons from hadronic matter (HM) for modified and unmodified ρ meson. Scenario (a) has been used for EoS.

the pole as well as in the continuum part of the spectral function, evaluated with and without the modified ρ spectral function discussed in Section 2 for RHIC. The enhancement in the region $0.1 \leq M \leq 0.7$ GeV is purely a medium effect and is a contribution from the Landau cut of the $\pi - \omega, h_1, a_1$ loops. In simple terms, the yield in this region results from the scattering of the ρ with thermal ω, h_1, a_1 and pions [14]. As seen from Eq. (26) these contributions are weighted by the Bose distribution functions for the pions (minus a much smaller contribution from the heavy mesons). In contrast, the vacuum spectral function naturally starts from the $2m_\pi$ threshold coming from the unity in the unitary cut contribution. The (small) kink at 0.42 GeV in this curve is due to the $3m_\pi$ threshold for ω production. The enhancement in the yield due to medium effects is ~ 20 for M around 400 MeV. Next we show in Fig. 6 the dependence of the yield from the two phases on the EoS. Dilepton radiation from hadronic phase outshines the emission from quark matter for M up to ϕ mass. Since we have included the continuum in the ρ and ω channels we ignore the four pion annihilation process [45] to avoid double counting. The contributions from quark matter phase dominates over its hadronic counter part for both the EoS for M beyond ϕ -peak. This fact may be used to extract various properties *i.e.* *average flow, temperature etc.* of quark matter and hadronic matter by selecting M windows judiciously. The dilepton yield from hadronic matter is observed to be larger when the HRG EoS is employed in comparison to LQCD. This can be understood in terms of the velocity of sound $v_s^2 (= dP/de$ evaluated at constant entropy) which controls the rate of expansion. For EoS of the type (a) $v_s^2 \sim 1/3$ in the QGP phase which is larger than the value of the corresponding quantity for EoS of the type (b). Therefore, the rate of expansion in the scenario (b) is comparatively slower, allowing the QGP to emit lepton pairs for a longer time resulting in greater yield for LQCD EoS. In contrast, for the EoS (a), the lower value of v_s for the hadronic phase results in a slower

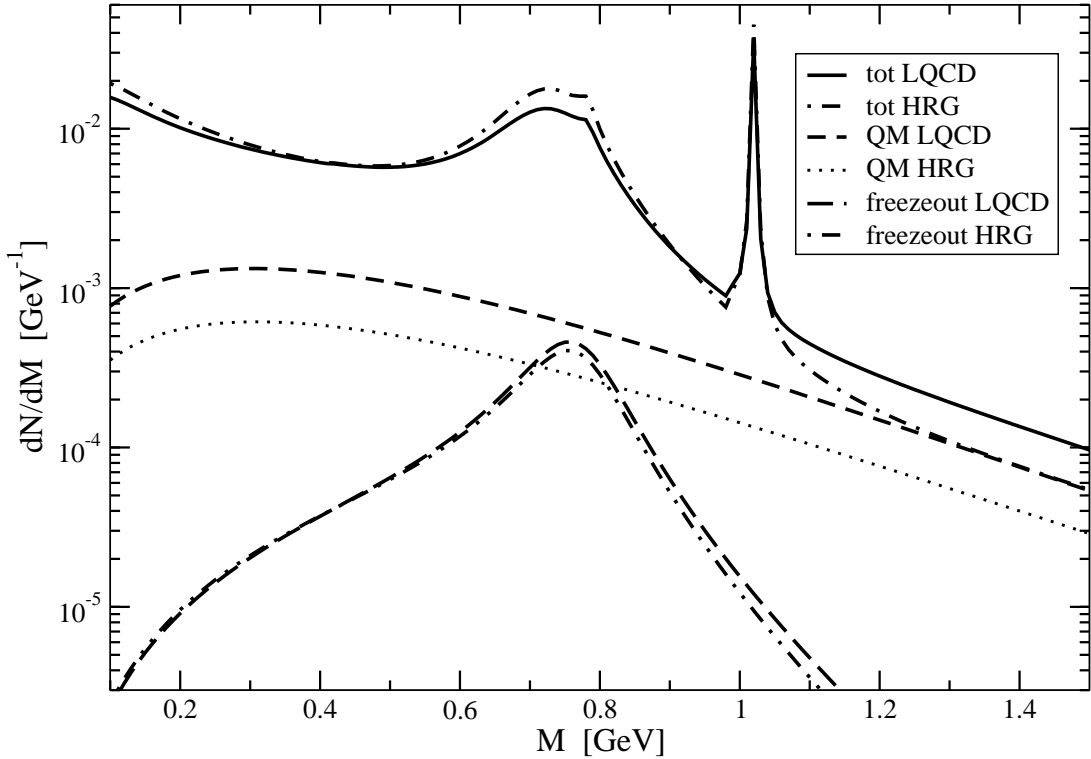


Figure 6: The invariant mass distribution of lepton pairs for RHIC initial condition with HRG and LQCD EoS.

cooling and hence a larger yield. Also shown for comparison is the yield from the decays of ρ mesons at the freeze-out for the two types of EoS used. The yield from this source is much smaller and we will not consider it any further.

Since the M spectra is invariant under flow we now turn to the $M_T (= \sqrt{p_T^2 + M_{av}^2})$ spectra to study this aspect. Fig. 7 shows the M_T spectra of lepton pairs at RHIC energies. Here the differential yield is integrated over small bins of the pair invariant mass (from M_1 to M_2) and plotted against $M_T - M_{av}$ which is actually a measure of the average kinetic energy (KE) of the pair, M_{av} being the average mass ($= [M_1 + M_2]/2$) of the bin. The average value of M_T for a static system at a temperature T is given by $\langle M_T \rangle \sim M + T$. Therefore, the average KE $\sim T$, is the slope of the M_T distribution. Initially, the entire energy of the system formed in HIC is thermal in nature and with progress of time some part of the thermal energy gets converted to the collective (flow) energy. In other words, during the expansion stage the total energy of the system is shared by the thermal as well as the collective degrees of freedom. As a consequence, unlike the invariant mass spectra, the M_T (or p_T) spectra is heavily influenced by the collective flow and the average KE or the inverse slope may be written as $T_{eff} = T + 1/2 M_{av} v_T^2$, where v_T is the average radial flow velocity. The M_T spectra of dileptons for various M -bins have an exponential nature, the inverse slope providing an effective temperature, T_{eff} . It is important to mention at this point that for a radially expanding system the T_{eff} has an explicit (linear) M dependence as mentioned above. However, it has also an implicit M dependence even when $v_T = 0$ (*i.e.* with longitudinal expansion only) because it is expected that the high (low) M pairs predominantly emit from the high (low) temperature or early (late) time zone. For a radially expanding system the M dependence of the T_{eff} is stronger than for a system which expands longitudinally only.

In Fig. 8 we have plotted the effective temperature versus M_{av} for various mass windows of the lepton

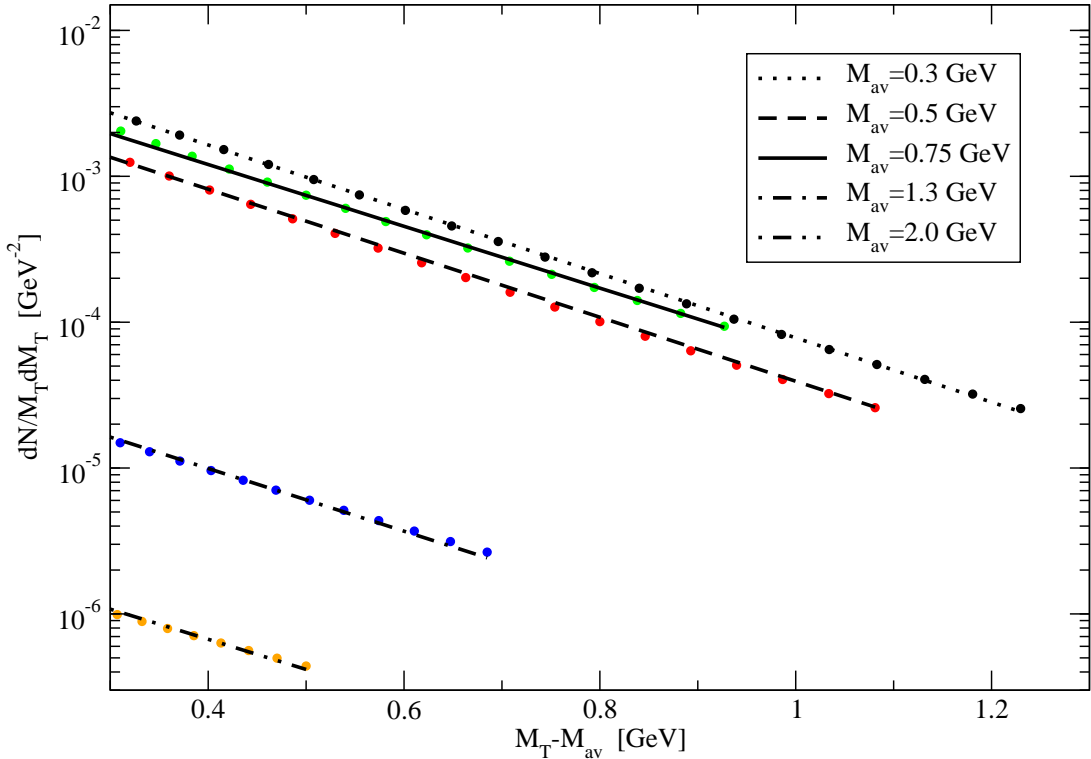


Figure 7: The dilepton yield plotted against $M_T - M_{av}$ for different M windows for RHIC initial conditions.

pairs at RHIC energies, evaluated with the in-medium spectral function of the vector mesons. Also shown by a filled square is the value of T_{eff} for the vacuum case in the window $0.4 \leq M \leq 0.6$ where there is substantial difference between the yields in free and medium cases as seen in Fig 5. The slope of these curves measure the average temperature and the flow of the matter.

Let us try to understand the non-monotonic variation of the inverse slope with M_{av} depicted in Fig. 8. In Fig. 6 it is shown that the high M (above ϕ peak) pairs originate predominantly from the partonic source and the low M (below ρ mass) domain, although outshine by the radiation from hadronic source, contains non-negligible contributions from quark matter *i.e.* the low M region contains contributions both from the hadronic as well as QGP phases. Now, the collectivity (or flow) in the system does not develop fully in the QGP because of the small life time of this phase which means that the radial velocity extracted from the high M region is small. Here the temperature decreases mainly due to longitudinal expansion and consequently, the effective slope decreases slowly with decreasing M_{av} . In contrast, the lepton pairs with mass around ρ -peak dominantly originate from the hadronic source (which appears in the late stage of the evolving system) and are significantly affected by the flow resulting in higher values of v_T and hence a higher T_{eff} . At still lower values of $M (< m_\rho)$ the contributions from hadronic phase is considerable. Therefore, the M_T spectra in this domain is affected by the flow significantly *i.e.* the value of v_T is large but can not be as large as in the ρ -peak region despite the substantial medium induced enhancement of the hadronic sources since this domain also contains contribution from the QGP. But for low $M (< m_\rho)$ the T_{eff} is smaller compared to the ρ peak region because of the smaller values M . The value of T_{eff} increases linearly with M up to the ρ peak, a behaviour typical of inverse slope extracted from the transverse momentum spectra of hadrons with different masses. Thus the values of T_{eff} for M below and above the ρ -peak are smaller compared to the values around the ρ peak even

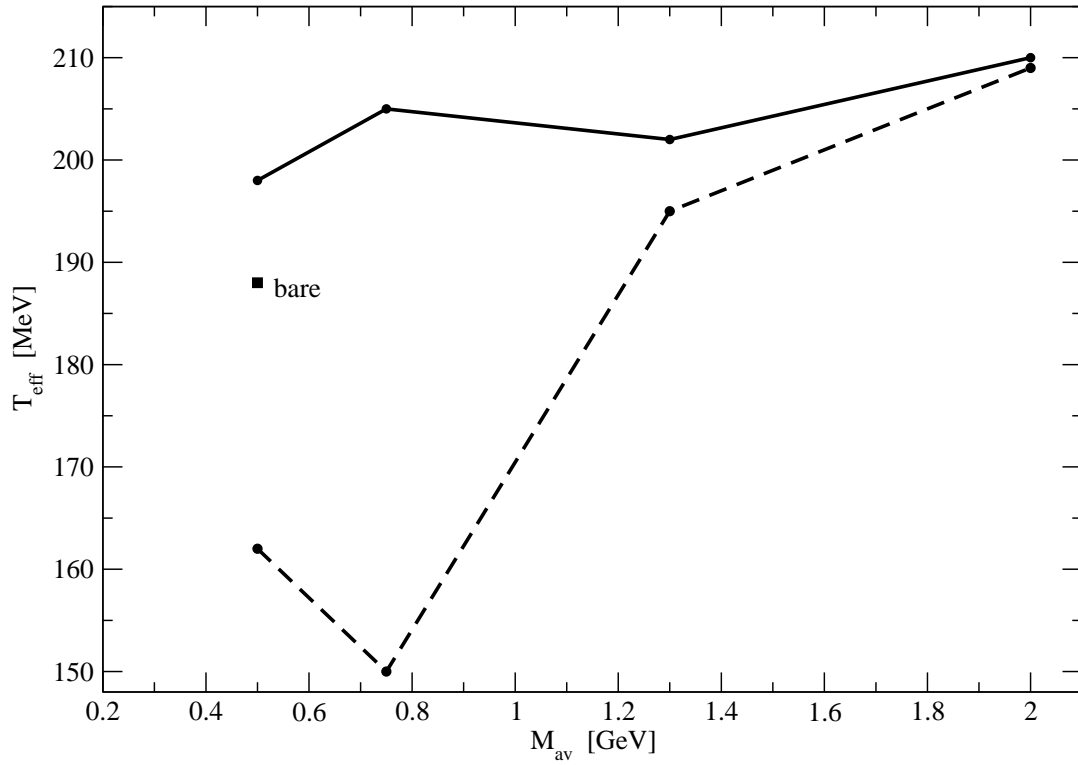


Figure 8: (Colour online) T_{eff} for different values of the M -bins for RHIC energy. The dashed line is obtained by setting $v_T = 0$.

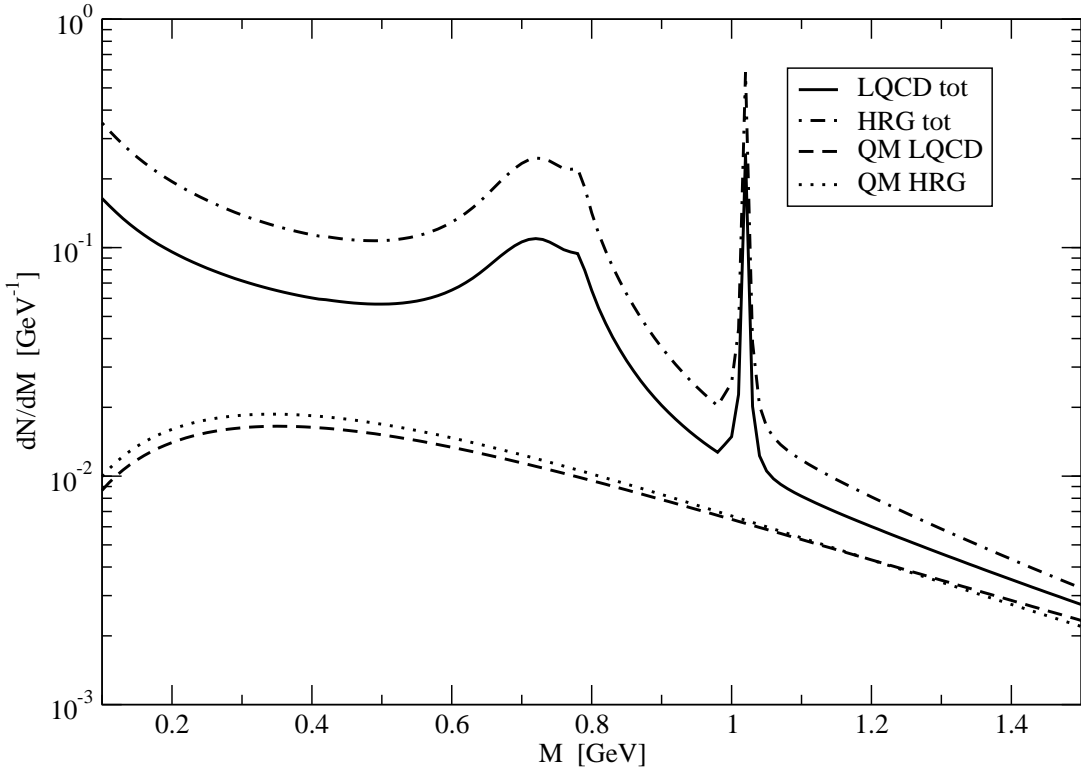


Figure 9: Dilepton yields for HRG EoS and LQCD EoS. The initial condition is taken for LHC energy.

in the presence of medium effects, resulting in the non-monotonic behaviour as displayed in Fig. 8, for $0.5 < M(\text{GeV}) < 1.3$.

The slope of the M_T spectra is connected with the average collective flow. It is well known that the average magnitude of radial flow at the freeze-out surface can be extracted from the p_T spectra of the hadrons. However, hadrons being strongly interacting objects can bring the information of the state of the system when it is too dilute to support collectivity *i.e.* the parameters of collectivity extracted from the hadronic spectra are limited to the evolution stage where the collectivity ceases to exist. These collective parameters have hardly any information about the interior of the matter. On the other hand the dileptons are produced and emitted from all space time points. Therefore, the value of v_T estimated from the dilepton spectra will be lower than the value extracted from the hadronic spectra [46]. Indeed, the values of v_T estimated from the slopes of the curve is 0.25 for the M domains $0.5 < M(\text{GeV}) < 0.77$. This value is much smaller than the value of v_T extracted from the hadronic spectra [47]. The dashed line in Fig. 8 is obtained by setting $v_T = 0$. The results indicate that the observed (solid line) rise (for $0.5 < M(\text{GeV}) < 0.77$) and fall (for $0.77 < M(\text{GeV}) < 1.3$) are due to radial expansion of the system. However, the rise in large M domain is due to cooling of the system due to longitudinal expansion - which is described as the implicit M dependence of T_{eff} above.

The invariant mass spectra of lepton pairs is displayed for LHC initial conditions in Fig. 9. Although, the results are qualitatively similar to RHIC, quantitatively the yield at LHC is larger. This is because of the larger four-volume of the system to be realised at LHC resulting from a higher value of T_i for fixed T_c and T_F . Similar kind of enhancement is also reflected in the transverse mass distributions of the lepton pairs at LHC (Fig. 10).

Finally the variation of inverse slope of the M_T distributions with M_{av} for LHC is depicted in Fig. 11. The values of T_{eff} for various M -bins are larger than RHIC because of the combined effects of large initial

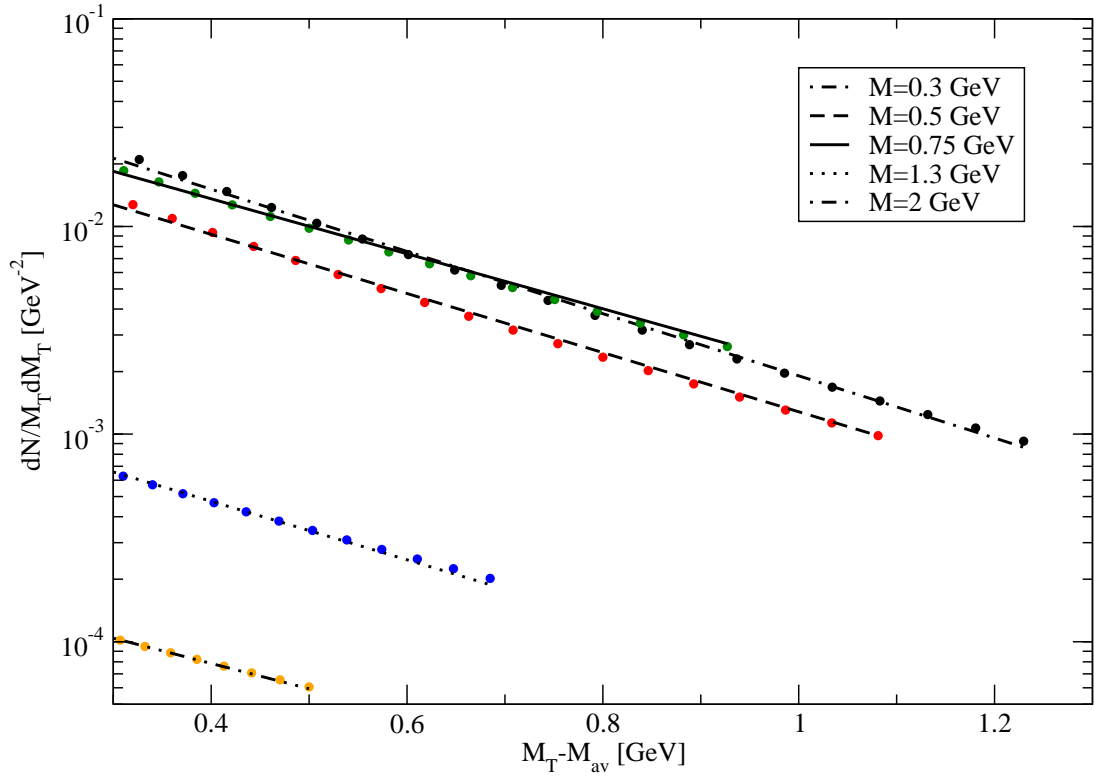


Figure 10: (Colour Online) The dilepton yield plotted against $M_T - M_{av}$ for different M windows for LHC initial condition.

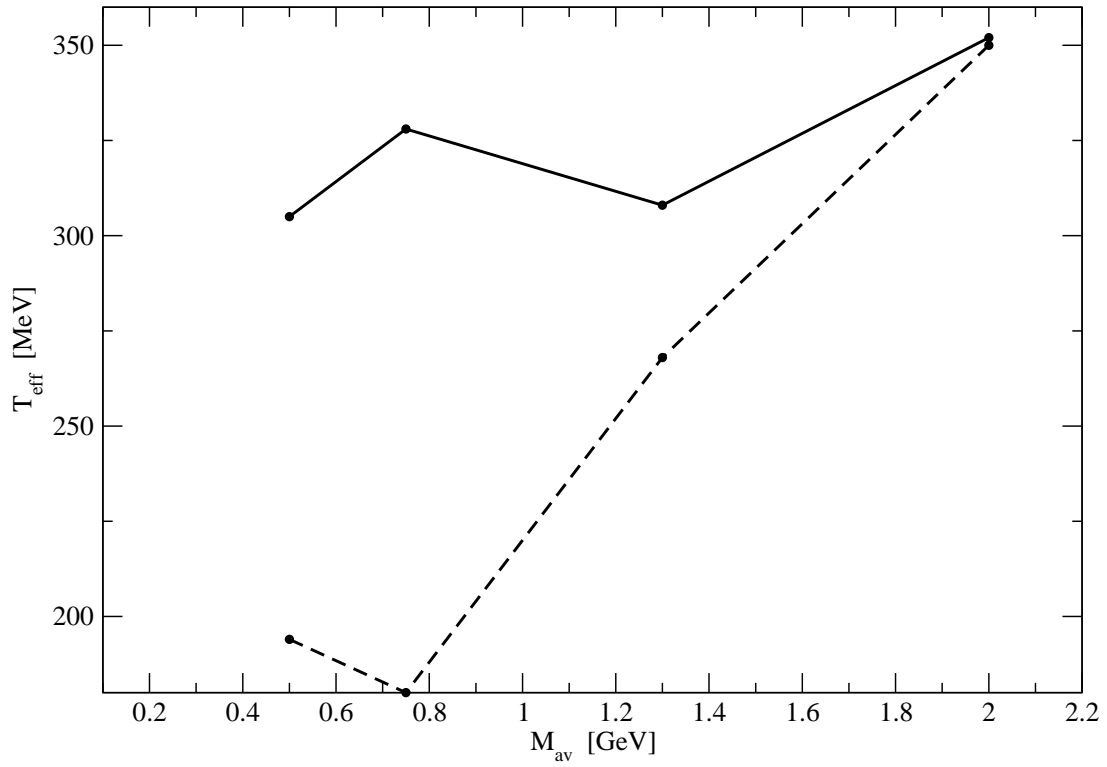


Figure 11: T_{eff} for different values of the M -bins for LHC conditions. The dashed line is obtained by setting $v_T = 0$.

temperature and flow. In fact the value of v_T for $0.5 < M(\text{GeV}) < 0.77$ is ~ 0.52 compared to 0.25 at RHIC. The radial flow in the system is responsible for the rise and fall of T_{eff} with M_{av} (solid line) in the mass region ($0.5 < M(\text{GeV}) < 1.3$), for $v_T = 0$ (dashed line) a completely different behaviour is obtained. This type of non-monotonic variation of T_{eff} can not be obtained with a single dilepton source [48]. Therefore, such non-monotonic variation of the inverse slope deduced from the transverse mass distribution of lepton pairs with average invariant mass is an indication of the presence of two different phases during the evolution of the system. Thus, such variation may be treated as a signal of QGP formation in heavy ion collisions. A comment on the thermal emission rate from the QGP is in order here. We have considered the lowest order processes to evaluate the the lepton pair productions from QGP. However, we have checked that the inclusions of the processes of order $O(\alpha_s)$ [49, 50, 51] changes the slope parameter, T_{eff} at low M by negligible amount. It is less than 1% for $M \sim 0.3$ GeV and at higher M it is vanishingly small.

The other sources of dileptons *e.g.* from the Drell-Yan (DY) mechanism and charm decays may provide significant “background” to the thermal productions at high mass region ($2 \leq M$ (GeV) ≤ 6 [52]) which are neglected here because in the present work we focus mainly on the low mass regions. Moreover, the contributions from the DY process and charm decays from proton+proton (pp) collisions may be used to estimate the similar contributions from heavy ion collisions at the same colliding energy by appropriately scaling pp data by the effective number of nucleon+nucleon collisions in nuclear interaction. The contributions from the ρ at the freeze-out surface has been evaluated and it is found to be small.

5 Conclusion

In this work we have attempted to bring out distinguishing features stemming from many body effects in the lepton pair yield from relativistic heavy ion collisions. On the microscopic side we have used a ρ spectral function evaluated at finite temperature in the framework of real time formalism of thermal field theory using interaction vertices from chiral perturbation theory. The effect of baryons have also been included in the empirical approach of Ref. [28] using resonance dominance in the forward scattering amplitude. A significant enhancement of the dilepton yield in the region below the nominal ρ peak has been obtained from the combined effect of mesons and baryons. The space-time evolution of the dilepton emission rate using relativistic hydrodynamics with chemical freeze-out reflects this enhancement in the invariant mass spectra.

On the macroscopic side, it is argued that the non-monotonic variation of the inverse slope deduced from the transverse mass distribution of lepton pairs for various values of the average invariant mass is an indication of the presence of two different phases during the evolution of the system. Thus, such a variation may be treated as a signal of QGP formation in heavy ion collisions.

Acknowledgement: JA’s research is partially supported by DAE-BRNS project No. 2005/21/5- BRNS/2455.

References

- [1] I. Arsene *et al.* (BRAHMS Collaboration), Nucl. Phys. A **757**, 1 (2005); B. B. Back *et al.* (PHOBOS Collaboration), Nucl. Phys. A **757**, 28 (2005); J. Adams *et al.* (STAR Collaboration), Nucl. Phys. A **757**, 102 (2005); K. Adcox *et al.* (PHENIX Collaboration), Nucl. Phys. A **757**, 184,(2005).
- [2] S. S. Adler *et al.* (PHENIX Collaboration), Phys. Rev. Lett. **96**, 202301 (2006); J. Adams *et al.* (STAR Collaboration), Phys. Rev. Lett. **91**, 072304 (2003). B. I. Abeleb *et al.* (STAR Collaboration), Phys. Rev. Lett. **98**, 192301 (2007); S. S. Adler *et al.* (PHENIX Collaboration), Phys. Rev. Lett. **96**, 032301 (2006).

- [3] A. Adare *et al.* [PHENIX Collaboration], Phys. Rev. Lett. **98**, 162301 (2007); B. I. Abelev *et al.* [STAR Collaboration], Phys. Rev. C **77**, 054901 (2008).
- [4] R. Arnaldi *et al.* for the NA60 collaboration, Phys. Rev. Lett. **100** 022302 (2008).
- [5] R. Rapp and J. Wambach, Adv. Nucl. Phys. **25**, 1 (2000)
- [6] G. Agakichiev *et al.* (CERES Collaboration) Phys. Lett. B **422**, 405 (1998).
- [7] S. Sarkar, J. Alam and T. Hatsuda, J. Phys. G **30**, 607(2004).
- [8] H. van Hees and R. Rapp, Nucl. Phys. A **806**, 339 (2008).
- [9] J. Ruppert, C. Gale, T. Renk, P. Lichard and J. I. Kapusta, Phys. Rev. Lett. **100**, 162301 (2008).
- [10] A. Adare *et al.* [PHENIX Collaboration], Phys. Rev. C **81**, 034911 (2010).
- [11] K. Dusling and I. Zahed, Nucl. Phys. **A825**, 212 (2009).
- [12] E. L. Bratkovskaya, W. Cassing and O. Linnyk, Phys. Lett. B **670** (2009) 428
- [13] A. Drees, Nucl. Phys. A **830**, 435c (2009).
- [14] S. Ghosh, S. Mallik and S. Sarkar, Eur. Phys. J. C **70** (2010) 251.
- [15] R. Rapp and C. Gale, Phys. Rev. C **60**, 024903 (1999).
- [16] J. Alam, S. Sarkar, P. Roy, T. Hatsuda and B. Sinha, Ann. Phys. **286**, 159 (2000).
- [17] P. Huovinen, P. V. Ruuskanen and J. Sollfrank, Nucl. Phys. **A650** (1999) 227.
- [18] M. Luzum and P. Romatschke, Phys. Rev. C **78** (2008) 034915 [Erratum-ibid. C **79** (2009) 039903]
- [19] J. Deng, Q. Wang, N. Xu and P. Zhuang, arXiv:1009.3091 [nucl-th].
- [20] L. D. McLerran and T. Toimela, Phys. Rev. D **31** (1985) 545.
- [21] J. Cleymans, J. Fingberg and K. Redlich, Phys. Rev. D **35**, 2153 (1987).
- [22] E. V. Shuryak, Rev. Mod. Phys. **65** (1993) 1.
- [23] M. Le Bellac, *Thermal Field Theory*, Cambridge University Press, (2000).
- [24] S. Mallik and S. Sarkar, Eur. Phys. J. C **61**, 489 (2009)
- [25] H. Nagahiro, L. Roca and E. Oset, Eur. Phys. J. A **36** (2008) 73
- [26] C. Amsler *et al.* [Particle Data Group], Phys. Lett. B **667**, 1 (2008).
- [27] R. Rapp, G. Chanfray and J. Wambach, Nucl. Phys. A **617** (1997) 472
- [28] V. L. Eletsky, M. Belkacem, P. J. Ellis and J. I. Kapusta, Phys. Rev. C **64** (2001) 035202
- [29] R. Rapp, J. Phys. G **34** (2007) S405

- [30] H. van Hees and R. Rapp, Phys. Rev. Lett. **97** (2006) 102301
- [31] R. A. Schneider and W. Weise, Phys. Lett. B **515**, 89 (2001)
- [32] J. K. Nayak, J. Alam, T. Hirano, S. Sarkar and B. Sinha, arXiv:0902.0446 [nucl-th].
- [33] H. von Gersdorff, M. Kataja, L. McLerran and P. V. Ruuskanen, Phys. Rev. **D34** 794; *ibid.* **D34** (1986).
- [34] J. D. Bjorken, Phys. Rev. D **27**, 140 (1983).
- [35] C. Bernard *et al.*, Phys. Rev. D **75** (2007) 094505.
- [36] R. C. Hwa R C and K. Kajantie, Phys. Rev. **D32**, 1109 (1985).
- [37] D. Khazreev and M. Nardi, Phys. Lett. **B507**, 121 (2001)
- [38] K. Aamodt *et al.* (for ALICE collaboration), Eur. Phys. J. C **68**, 89 (2010).
- [39] J. Alam, J. K. Nayak, P. Roy, A. K. Dutt-Mazumder and B. Sinha, J. Phys. G **34**, 871 (2007); B. K. Patra, J. Alam, P. Roy, S. Sarkar and B. Sinha, Nucl. Phys. A **709**, 440 (2002).
- [40] P. Braun-Munzinger, K. Redlich and J. Stachel in Quark Gluon Plasma 3, R. C. Hwa and X. N. Wang (Eds.), World Scientific Publishing, Singapore, 2003.
- [41] H. Bebie, P. gerber, J. L. Goity and H. Leutwyler, Nucl. Phys. B **378**, 95 (1992).
- [42] T. Hirano and K. Tsuda, Phys. Rev. C **66** (2002) 054905.
- [43] F. Cooper and G. Frye, Phys. Rev. D **10** (1974) 186.
- [44] K. Dusling and I. Zahed, Phys. Rev. C **80**, 014902 (2009).
- [45] P. Lichard and J. Juran, Phys. Rev. D **76**, 094030 (2007)
- [46] S. Damjanovic, J. Phys. G **35**, 104036 (2008).
- [47] X. Nu and M. Kaneta, Nucl. Phys. A **698**, 306c (2002).
- [48] T. Renk and J. Ruppert, Phys. Rev. C **77**, 024907 (2008).
- [49] E. Braaten, R. D. Pisarski and T. C. Yuan, Phys. Rev. Lett. **64**, 2242 (1990).
- [50] M. H. Thoma and C. T. Traxler, Phys. ReV. D **56** (1997) 198.
- [51] T. Altherr and P. V. Ruuskanen, Nucl. Phys. B **380** (1992) 377.
- [52] R. Vogt, B. V. Jacak, P. L. McGaughey, P. V. Ruuskanen, Phys. Rev. D **49**, 3345 (1994).